Research Square

Preprints are preliminary reports that have not undergone peer review.
They should not be considered conclusive, used to inform clinical practice,
or referenced by the media as validated information.

A UDP-glycosyltransferase gene enhances resistance to Fusarium avenaceum in red clover

Shridhar Jambagi

shridhar.jambagi@slu.se

Swedish University of Agricultural Sciences

Aimer Gutierrez-Diaz

Swedish University of Agricultural Sciences

Christina Dixelius

Swedish University of Agricultural Sciences

Research Article

Keywords: Fusarium avenaceum, receptor-like kinase, root rot, Trifolium pratense, UDP-glycosyltransferase

Posted Date: September 16th, 2026

DOI: https://doi.org/10.21203/rs.3.rs-10825234/v1

License: This work is licensed under a Creative Commons Attribution 4.0 International License.
Read Full License

Additional Declarations: No competing interests reported.

Abstract

Root rot is an important red clover disease caused by *Fusarium avenaceum*. Severe attacks significantly reduce the persistence of this forage crop. In this study, we used contrasting accessions to identify important defense factors against the *F. avenaceum* pathogen initially using RNA-seq. We identified 251 genes that were uniquely induced in the more resistant accession Formica, including several receptor-like kinases and UDP-glycosyltransferases. Four candidates were shortlisted on the basis of their expression patterns and predicted defense-related functions for further evaluation in a new transient expression assay using red clover leaves. *TpUGT89B1* and *TpLRR-RLK* most effectively reduced fungal colonization and were subsequently used in stable transformation in the background of the susceptible accession SW 1678002. Constitutive expression of either *TpUGT89B1* or *TpLRR-RLK*significantly enhanced resistance to *F. avenaceum*, with *TpUGT89B1*providing the greatest reduction in fungal biomass and disease symptoms. Sequence comparison and structural modeling revealed that TpUGT89B1 possesses the conserved GT-B fold and characteristic features of a plant family 1 UDP-glycosyltransferase. Homology-based STRING analysis, supported by RT—qPCR, revealed that TpUGT89B1 is involved in flavonoid biosynthesis through its co-expression with *TpCHS*, *TpCYP75B1* and *TpFLS1*. Collectively, the results of this study provide integrated transcriptomic information and structural prediction of TpUGT89B1, suggesting that it functions in defense through glycosylation-associated specialized metabolism.

Key message

Comparative transcriptomics combined with transient and stable transformation revealed that *TpUGT89B1* is a defense gene that restricts *Fusarium avenaceum* colonization in red clover.

Introduction

Fabaceae, formerly Leguminosae, is among the largest and most diverse plant families in the world, with more than 19,000 species divided into approximately 750 genera (The Legume Phylogeny Working Group 2018). Many legume species are economically important and are used for oils, fuel and timber in addition to a wide range of agricultural products (Gresshoff et al. 2015; Lisciani et al. 2024). Red clover (*Trifolium pratense*) is an important perennial forage crop in temperate regions. This legume is a strict outcrossing species carrying incompatibility alleles, a feature that has generated populations with high levels of heterozygosity (Jones et al. 2020). This is a reality that has both negative and positive consequences for breeders working with crop improvements. In addition to animal feed products, red clover generates numerous environmental and socio-economic benefits, where the atmospheric nitrogen fixation capacity constitutes a cornerstone, not least in sustainable agricultural systems and organic food production (Valujeva et al. 2025).

Rhizobia is the best-known group of symbiotic nitrogen-fixing bacteria and belongs to alpha-proteobacteria, a bacterial class with a constantly changing taxonomy (Rajkumari et al. 2022). Root

nodules have been studied for many years, with emphasis on the symbiotic relationship between host plants and nodule-forming bacteria (Schultze and Kondorasi 1998; Nuc and Olejnik 2025.) Within the nodules, atmospheric nitrogen is fixed by the bacteria and reduced in a process catalyzed by the nitrogenase enzymatic complex to a form that can be assimilated by the plant (Poole et al. 2018). In exchange for nitrogen, the plant supports the bacteria with carbohydrates. Nitrogen fixation is mainly controlled by the bacterial genes encoding *nod*, *nif* and *fix*. Other important factors in nodules are energy, carbon and nitrogen metabolism and their regulation. On the plant side, it is thought that fine-tuned regulation of innate immunity is required throughout rhizobial infection, symbiotic establishment, and maintenance (Cao et al. 2017). Processes comprising symbiotic nitrogen fixation have been dissected in detail (Lindström and Mousavi 2020; Kundu et al. 2025). It is therefore crucial for plants to discriminate between beneficial and pathogenic microbes (Poole et al. 2018; Ngou et al. 2022; Grundy et al. 2023).

In a study aimed at mapping the red clover root microbiota in Sweden, it was found that microbial community composition was shaped mainly by geographic location and management procedures (Jambagi et al. 2023). *Rhizobium leguminosarum* bv. *trifolii* was negatively associated with all fungal pathogenic taxa recognized in the collected samples. Sixty-two potential pathogenic fungi were identified, among which the root rot pathogen *Fusarium avenaceum* was present. This global fungus causes root rot or blights on diverse plant species and produces toxins on cereal grains, which can be explained by enriched genes encoding secondary metabolites in its genome (Lysøe et al. 2014). The fungus is also part of the Fusarium head blight complex in cereals, particularly in Europe and Canada, where it contributes to disease severity (Nielsen et al. 2014; Xue et al. 2019). Unlike *Fusarium graminearum*, which primarily relies on trichothecene mycotoxins during infection, *F. avenaceum* produces a diverse array of secondary metabolites, many of which possess phytotoxic or antimicrobial activities that may contribute to disease development (Inbaia et al. 2023). However, the molecular mechanisms through which red clover recognizes and responds to *F. avenaceum* infection have not been studied previously.

In the present work, comparative RNA-seq of contrasting red clover accessions was performed to identify defense genes against *F. avenaceum*. An *Agrobacterium*-mediated transient expression system was established using a susceptible red clover breeding population to identify important defense genes from a list of predicted candidates. Next, two genes were prioritized for functional analysis using a stable transgenic approach. *TpUGT89B1*, encoding a putative family 1 uridine 5'-diphosphate glycosyltransferase (UGT), is involved in several important metabolic pathways, including the detoxification of fungal-derived compounds (Wang et al. 2009). *TpLRR-RLK*, encoding a leucine-rich repeat receptor-like kinase, is a family known to be cell-surface receptors involved in pathogen recognition and the sensing of external signals that are further transmitted to the interior of the plant cell (Chakraborty et al 2019). Comparative transcriptomics, transient and stable expression analyses, structural modeling and expression profiling revealed that *TpUGT89B1* was the strongest defense gene candidate in our datasets. *TpLRR-RLK* may function as an additional component in this defense system against *F. avenaceum* in red clover.

Materials and Methods

Fungal strain and inoculum preparation

The *F. avenaceum* CBS 115699 strain, obtained from the Westerdijk Fungal Biodiversity Institute, The Netherlands, was maintained on potato dextrose agar (Sigma—Aldrich, USA) at 21°C in the dark. For sporulation, 5 mm mycelial plugs from 5-day-old actively growing cultures were transferred onto V8 media plates and incubated at 21°C for 10 d under UV light (350–400 nm). Conidia were harvested by flooding the plate surface with 10 ml of sterile distilled water, gently scraping the colony surface with a sterile spreader, and filtering the suspension through sterile Miracloth (Millipore, USA) to remove mycelial fragments. concentration was determined using a hemocytometer and adjusted to 1 x 10^6 conidia/ml. The virulence of the fungus was maintained by regular inoculation of 3-week-old sterile red clover seedlings and re-isolation of the fungi protruding from the root tissues, followed by cultivation on potato dextrose agar plates.

Red clover materials

Red clover accessions showing contrasting responses to *F. avenaceum* (Jambagi and Dixelius 2023) were selected for transcriptomic analysis. The most resistant accession, Formica, and the most susceptible population, SW 1678002, were chosen for RNA-seq experiments (hereafter referred to as resistant and susceptible red clover). Fungal-infected and non-infected root materials generated through hydroponic screening were used for RNA extraction. Briefly, three-week-old plants were inoculated with an *F. avenaceum* spore suspension (~30 000 spores/ml), while control plants were mock-inoculated with sterile water. Root samples were collected 7 days post-inoculation (dpi), rinsed thoroughly with sterile water and patted dry on a clean paper towel. Roots from three individual plants were pooled, snap-frozen in liquid nitrogen and stored at -70°C until RNA extraction. Three biological replicates for each treatment (infected vs. non-infected) were prepared for RNA-seq analysis.

RNA extraction and sequencing

Total RNA was extracted from ~100 mg of root tissue using the Spectrum Plant Total RNA Kit (Sigma—Aldrich, USA) according to the supplier's instructions. RNA integrity was measured using an Agilent 2100 Bioanalyzer (Agilent Technologies, Inc., Germany). Samples with RIN values ≥ 8.0 were used for RNA-seq. Three biological replicates of each genotype and treatment were submitted to the National Genomics Infrastructure (NGI) sequencing facility (SciLife Laboratory, SNP&SEQ Technology Platform, Uppsala, Sweden) for library preparation using the Illumina TruSeq Stranded mRNA polyA selection kit and sequenced on a NovaSeq S6000 S4 flow cell with 150 bp paired-end reads.

RNA-seq data analysis

The raw sequence data were processed using the reproducible Nextflow nf-core/rnaseq pipeline (v3.8.1) (Di Tommaso et al. 2017). Adapter sequences and low-quality bases were removed using Trim Galore! with Cutadapt (Martin 2011). Filtered reads were aligned to the *T. pratense* reference genome (De Vega et al. 2015) using STAR (Dobin et al. 2013), and transcript abundance was quantified with Salmon (Patro et al. 2017) and expressed as transcripts per million (TPM). A quality assessment of the sequencing data was performed using MultiQC (Ewels et al. 2016). Differential gene expression analysis was carried out using DESeq2 (Love et al. 2014). Genes with a false discovery rate (FDR) < 0.01 and a $|\log_2$fold change ≥ 1 were considered significantly differentially expressed. Principal component analysis was performed using normalized TPM values. Venn diagrams were generated using http://bioinformatics.psb.ugent.be/webtools/Venn/ to identify genes that were uniquely or commonly expressed. The functional annotation was based on the *T. pratense* genome annotation (De Vega et al. 2015). Unannotated genes were further analyzed using the NCBI non-redundant protein database, PLAZA v5.0 (Van Bel et al. 2012) and UniProtKB/Swiss-Prot (Boutet et al. 2016).

Candidate gene selection

From a list of 50 DEGs (Table S1), four candidates were shortlisted for follow-up analysis. The selection criteria included statistically significant (FDR < 0.01) $\log_2$fold change values and functional annotation relevant to disease defense, pathogen recognition, or detoxification pathways. Genes of unknown function with putative defense roles were also considered. The selected genes with the following predicted functions were *TpUGT89B1* (Tp57577_TGAC_v2_gene36361), which plays roles in secondary metabolite modification and mycotoxin detoxification; *TpLRR-RLK* (Tp57577_TGAC_v2_gene1430), encoding a leucine-rich repeat receptor-like serine/threonine kinase involved in pathogen recognition; *TpLecRLK9* (Tp57577_TGAC_v2_gene29843), encoding an L-type lectin-domain receptor kinase IX.1-like protein implicated in plant immune responses; and one uncharacterized gene, *Tp11408* (Tp57577_TGAC_v2_gene11408), showing strong pathogen-induced expression.

Plasmid construction

Total RNA was isolated from Formica roots using a RNeasy Plant Mini Kit (Qiagen Sciences Inc., USA), and DNA was treated with DNase I (Thermo Fisher Scientific, USA). cDNA was synthesized using a Maxima First Strand cDNA Synthesis Kit (Thermo Fisher Scientific, USA). To generate gene constructs, cDNA target sequences were amplified via PCR with Phusion DNA polymerase (Thermo Fisher Scientific, USA) using an attB gene-specific primer set. The amplified fragments were individually cloned and inserted into the entry vector using Gateway BP Clonase II Enzyme (Invitrogen, Thermo Fisher Scientific, USA). Single-colony plasmids were purified, and the plasmid DNA was restricted, followed by Sanger sequencing. Confirmed inserts were introduced into suitable destination vectors using the Gateway system (Invitrogen, Thermo Fisher Scientific, USA). Finally, the *p35S:TpUGT89B1-GFP*, *p35S:TpLRR-RLK-GFP, p35S:TpLecRLK9-GFP* and *p35S:Tp11408-GFP* constructs were individually transformed into the

Agrobacterium tumefaciens strain AGL1. Information on all the primers and vectors used in this study is provided in Table S2.

Transient assay

AGL1 strains carrying the empty vector or the overexpression (OE) constructs were grown overnight in LB medium supplemented with 25 µg/ml rifampicin and 100 µg/ml spectinomycin. Bacteria were harvested by centrifugation, resuspended in infiltration medium (10 mM MES, pH 5.6, 10 mM MgCl2, and 100 µM acetosyringone) to an OD600 of 0.2, and incubated for 2 h at room temperature prior to leaf infiltration. Four-week-old red clover plants (SW 1678002) grown at 22°C under a 16 h photoperiod were used for leaf agroinfiltration. After infiltration, the plants were maintained in the dark for 24 h.

At 24 h post-infiltration, 100 µl of *F. avenaceum* spore suspension (10^6 spores/ml) was applied directly to the infiltrated leaf area. The plants were covered with transparent plastic bags to maintain high humidity and incubated in a growth chamber at 22°C under a 16 h photoperiod with a light intensity of 120 µmol m^{-2} s^{-1}. Phenotypic responses were monitored daily. The infiltrated leaf tissue was harvested at 5 dpi, snap-frozen in liquid nitrogen, and stored at − 70°C. Total DNA was extracted, and fungal biomass was quantified by qPCR as described in Jambagi and Dixelius (2023).

Agrobacterium-mediated transformation

The two candidate genes that most effectively reduced *F. avenaceum* colonization in the transient assay, *TpUGT89B1* and *TpLRR-RLK*, were selected for further investigation. To generate transgenic red clover lines, the *F. avenaceum*-susceptible red clover accession SW 1678002 was transformed with an *Agrobacterium* AGL1 strain carrying either *p35S:TpUGT89B1-GFP* or *p35S:TpLRR-RLK-GFP* using a method based on soybean (Li et al. 2017) with several modifications. Information about the different media is provided in Table S3. The seeds were surface-sterilized and germinated on MS medium supplemented with vitamins (Duchefa Biochemie, The Netherlands) (0.5% sucrose, 2.5 g/l phytagel) for 2 d under constant light. The hypocotyls from two-day-old plants were trimmed to a length of approximately 0.5–0.7 cm in liquid CCM (co-cultivation medium), rapidly transferred to CCM containing *Agrobacterium* AGL1 cells (OD = 0.3) and incubated for 30 min at room temperature. The hypocotyls were placed on solid CCM and left overnight at 28°C in a 24°C dark room.

After two days of co-cultivation, the explants were transferred to SIM (shoot induction medium). Explants were subcultured onto fresh SIM every 5–6 d for 3–4 weeks. Emerging shoots were transferred to M2 medium and subcultured weekly for 4–5 weeks until the roots developed and the shoots were elongated. Rooted plantlets were screened for the presence of the *NPTII* selection marker by PCR and then transferred to a hydroponic system for subsequent infection assays in a growth chamber at 22 ± 1°C with a 16 h photoperiod and 120 µmol m^{-2} s^{-1} light intensity (Jambagi and Dixelius 2023).

RNA isolation and real-time quantitative PCR (RT-qPCR)

Total RNA was isolated from the roots of the wildtype and red clover-OE lines using a Spectrum Plant Total RNA Kit (Sigma–Aldrich, USA) following the manufacturer's protocol. cDNA was synthesized with a Maxima First Strand cDNA Synthesis Kit (Thermo Fisher Scientific, Lithuania). RT–qPCR was performed with Maxima SYBR Green/Fluorescein qPCR Master Mix (Thermo Fisher Scientific, Lithuania). Gene-specific primers were designed using Primer-BLAST (Ye et al. 2012), and expression was normalized to that of the *translation initiation factor* (*EIF-4α*) gene in red clover (Mehdi Khanlou and Van Bockstaele 2012). Gene expression levels were quantified using the $2^{-\Delta\Delta Ct}$ method (Livak and Schmittgen 2001). Three independent OE lines were analyzed for each construct. For each OE line, roots from four individual transgenic plants were pooled to form one biological replicate, and three biological replicates were analyzed. Each RT–qPCR was performed with two technical replicates to ensure reproducibility.

Structural modeling and ligand docking

Structural modeling was performed to determine whether TpUGT89B1 possesses the conserved structural features of plant family 1 UGTs. TpUGT89B1 was modeled with Protenix under default settings (ByteDance AML AI4Science Team et al. 2025), a deep learning-based protein structure prediction model trained on experimentally resolved structures curated from the Protein Data Bank (PDB). The TpUGT89B1 protein sequence was searched against PDB integrated within Protenix to identify experimentally resolved structural homologs. UDP-2-fluoro-2-deoxy-D-glucose (U2F) and trichothecene scaffold (7E0) were specified as donor and acceptor ligands, respectively. Five structural models were generated and ranked by the interface-predicted template modeling score (ipTM), predicted template modelling score (pTM), per-residue local distance difference test (pLDDT), and global predicted distance error (GPDE) values reported by Protenix. Residue-pair predicted aligned error (PAE) and distance error (PDE) matrices, together with contact probability values, were extracted from the Protenix JSON output and collapsed into residue-level interface statistics by taking, for each residue, the minimum PAE, PDE and maximum contact probability. The predicted binding sites were interpreted using the experimentally resolved rice UGT Os79 in complex with UDP and trichothecene (Wetterhorn et al. 2016). The structural model, model confidence scores and scripts used for structural analysis are available in the GitHub repository https://github.com/AimerGDiaz/TpUGT89B1_Docking.

STRING-based network analysis and RT–qPCR validation

STRING analysis was conducted independently of structural modeling to identify biological pathways associated with TpUGT89B1. The protein sequence of TpUGT89B1 (NCBI accession: XP_045804762.1) was analyzed using the STRING database (v12.0; https://string-db.org), with *T. pratense* specified as the target species and a minimum interaction confidence score of 0.4 (Szklarczyk et al. 2025). Given that no direct interaction data were available for UGT89B1-like proteins in the red clover genome, a homology-based network analysis was performed using the proteomes of *Medicago truncatula* and *Arabidopsis thaliana*. The closest homologs were identified, and their predicted interaction networks were examined to identify biological pathways potentially associated with TpUGT89B1. Genes representing major

components of the predicted flavonoid biosynthesis pathway were selected for transcript analysis. The transcript levels of *TpUGT89B1*, *TpCHS*, *TpFLS1* and *TpCYP75B1* were determined by RT—qPCR using RNA isolated from infected and non-infected Formica roots collected at 7 dpi. The corresponding red clover orthologs were identified by BLASTP analysis.

Statistical analysis

At least three biological replicates for each treatment or plant material were used. Statistical differences were determined using Student's *t* test, except that one-way ANOVA and Tukey's multiple comparisons of means were applied for multiple group comparisons. The significance level was set at 95%.

Data availability

The transcriptome data generated in this study are available from the European Nucleotide Archive (ENA, https://www.ebi.ac.uk/ena/browser/search) under Bioproject "PRJEB123873". The ligand-bound structural model of TpUGT89B1 in interaction with 7E0 and U2F, together with the scripts used for downstream analyses, is available at https://github.com/AimerGDiaz/TpUGT89B1_Docking. Red clover materials are available from Linda.Ohlund@lantmannen.com. Other data generated or analyzed during this study are included in this article and its supplementary information files or are available from the corresponding author on reasonable request.

Results

UGT and RLK genes are highly elevated upon Fusarium avenaceum infection.

To identify defense gene candidates in red clover to *F. avenaceum*, RNA-seq analysis was performed on our most contrasting accessions Formica (R) and SW 1678002 (S). On average, the sequencing generated 50 million high-quality reads per sample, with more than 75% mapping efficiency to the red clover genome, representing enough sequence data for analyzing differential gene expression. Principal component analysis of the entire dataset revealed clear separation between infected and non-infected samples and between accessions, indicating distinct transcriptional reprogramming in response to *F. avenaceum* infection (Fig. 1A). Differential expression analysis identified both shared and accession-specific transcriptional responses to *F. avenaceum* infection (Fig. 1B, C). In the resistant Formica dataset, 251 genes were uniquely elevated, and 173 genes were uniquely downregulated following infection compared with those in the susceptible SW 1678002 dataset. Functional annotation revealed enrichment of genes involved in defense signaling, secondary metabolism, and detoxification and a substantial number of genes with unknown functions.

To identify candidate defense genes, subsequent analyses focused on transcripts that were uniquely induced in the resistant accession. The 50 most strongly elevated genes were examined in detail, with a particular emphasis on genes associated with defense-related functional categories (Table S1). A few UGTs are known to impact salicylic acid homeostasis in Arabidopsis (Bauer et al. 2021). In our datasets, genes associated with salicylic acid biosynthesis or signaling were not identified among the highly

activated transcripts. Several members of the *UGT* and *RLK* families were strongly induced in Formica. Three *UGT* genes, *TpUGT89B1*, *TpUGT85A2* (*Tp57577_TGAC_v2_gene29367*), and *TpUGT85A7* (*Tp57577_TGAC_v2_gene34750*), were strongly induced by infection. Similarly, several *RLK* genes representing different structural classes, including *LRR-RLKs*, *cysteine-rich receptor-like kinases* (*CRKs*), *L-type lectin-domain-containing RLKs* (*LecRLKs*), and *wall-associated receptor kinases* (*WAKs*), were strongly activated. Among these genes, *TpCRK* (Tp57577_TGAC_v2_gene10948), *TpLRR-RLK* and *TpLecRLK9* exhibited the strongest induction.

Based on transcript abundance and predicted biological function, four genes were selected to confirm their expression patterns by RT—qPCR: *TpUGT89B1*, *TpLRR-RLK*, *TpLecRLK9* and *Tp11408*. Although *TpCRK* was initially included among the candidates, repeated attempts to amplify its coding sequence were unsuccessful; therefore, it was excluded from further analysis. We selected one uncharacterized gene, *Tp11408*, to identify new candidates involved in *Fusarium* defense. Compared with the non-infected controls, all four genes exhibited strong pathogen-induced expression (Fig. S1, $P \leq 0.05$ or $P \leq 0.01$). The transcript patterns were consistent with the RNA-seq results, supporting the reliability of the transcriptomic dataset and the selection of these candidates for transient assays to evaluate their contribution to restricting fungal colonization.

TpUGT89B1 and TpLRR-RLK reduce F. avenaceum colonization in transient assays.

Nicotiana benthamiana plants were first used for transient assays but were found to be incompatible with *F. avenaceum* infection. Among our materials, SW 1678002 was most susceptible to the fungus (Jambagi and Dixelius 2023) and thus was examined for leaf responses. Compared with empty vector control, transient expression of *TpUGT89B1* significantly reduced lesion development following *F. avenaceum* inoculation (Fig. 2A, B, $P < 0.05$). A similar trend was found when *TpLRR-RLK* was tested but to a lesser extent than *TpUGT89B1* (Fig. 2A, B). The expression of *TpLecRLK9* similarly restricted fungal colonization; however, the effect was weaker than that observed for either *TpUGT89B1* or *TpLRR-RLK* (Fig. 2A, B). In contrast, *Tp11408* resulted in larger necrotic lesions and increased fungal biomass (Fig. 2A, B), indicating increased susceptibility to *F. avenaceum*.

TpUGT89B1 and **TpLRR-RLK confer enhanced protection against F. avenaceum**.

Based on the transient assay results, *TpUGT89B1* and *TpLRR-RLK* were selected for stable transformation experiments. The constitutive CaMV 35S promoter was used to prepare all the constructs, as amplification of the native red clover promoter regions was unsuccessful. The plant transformation efficiency, calculated as the percentage of PCR-confirmed independent transgenic plants recovered per 100 inoculated hypocotyl explants of SW 1678002, was 4.6% for *TpUGT89B1* and 6.6% for *TpLRR-RLK* (Table S4). Both *TpUGT89B1* and *TpLRR-RLK* transcript levels were significantly greater in the OE lines than in the wildtype SW 1678002 plants (Fig. 3A, $P \leq 0.05$ or $P \leq 0.01$).

Next, the responses of the transgenic lines to *F. avenaceum* were evaluated. After 7 dpi, the wildtype plants showed typical disease symptoms, including root browning, leaf chlorosis and reduced root

biomass. Plants overexpressing *TpUGT89B1* showed reduced disease symptoms and accumulated significantly less fungal DNA in the roots, with an approximately two-fold reduction in fungal biomass compared with the wildtype (Fig. 3B, C; $P < 0.05$). Plants overexpressing *TpLRR-RLK* also exhibited reduced disease severity and fungal biomass, however to a lesser extent (approximately 1.6-fold decrease in fungal DNA), and these plants displayed greater root discoloration and leaf chlorosis than the *TpUGT89B1* lines (Fig. 3B, C; $P < 0.05$). The transcript levels of both *TpUGT89B1* and *TpLRR-RLK* in the OE lines were also compared to those detected in *F. avenaceum*-infected Formica plants, and no significant differences were detected (Fig. S2). This observation suggests that the 35S promoter did not cause atypical high defense responses or other phenotypical artifacts.

TpUGT89B1 is predicted to adopt a canonical plant UGT fold capable of binding UDP-sugar donors and trichothecene-like acceptors.

Sequence comparison identified the rice glucosyltransferase Os79 as the closest experimentally characterized structural homolog in the PDB (Supplementary Data File 1). Os79 has been resolved in a complex with the UDP-glucose donor analog U2F and a trichothecene ligand (Wetterhorn et al. 2016), providing a structural reference for donor and acceptor binding regions. Structural modeling predicted that TpUGT89B1 adopts the conserved GT-B fold characteristic of plant family 1 UGT, with an N-terminal acceptor-binding region and a C-terminal UDP-sugar donor-binding domain (Fig. 4A). Protein—ligand docking revealed that the UDP-sugar analog U2F could be accommodated within the predicted conserved C-terminal donor binding pocket, whereas the reference trichothecene ligand 7E0 occupied the adjacent N-terminal acceptor binding pocket enriched in hydrophobic contacts (Fig. 4B; Fig. S3). Amino acid residues with contact probabilities greater than 0.5 at the predicted acceptor binding site included Ser129, Ala133, Ser137, Leu140, Ser174 and Ser176, with Ala376 and Asp377 from the donor binding pocket also contributing to ligand interactions (Fig. 4B; Fig. S3). The trichothecene ligand was used only as a structurally characterized reference molecule and does not imply that *F. avenaceum* produces trichothecenes. Superposition of the predicted TpUGT89B1 model with Os79 revealed conservation of the overall GT-B fold and the predicted donor- and acceptor-binding regions, supporting the structural capacity of TpUGT89B1 to recognize fungal-derived small molecules.

TpUGT89B1 is co-expressed with flavonoid biosynthesis genes during F. avenaceum infection

To explore the potential functional context of TpUGT89B1, homolog-based STRING analysis was performed. Five close homologs were identified in Medicago (A0A072TQ85, G7IT14_MEDTR, MTR_0009s0240, A0A072TSA1, A0A072UML8), of which only A0A072UML8, sharing 31.4% sequence identity with TpUGT89B1, showed a predicted functional association network. This network comprised 15 associated proteins supported primarily by co-expression and text-mining evidence (confidence scores of 0.464–0.727). Here, a group of proteins enriched in the phenylpropanoid and flavonoid biosynthesis pathways were identified (Table S5). The highest-confidence interactor of A0A072UML8 was leucoanthocyanidin dioxygenase (ANS; score 0.727), a 2-oxoglutarate iron-dependent oxygenase

that catalyzes the penultimate step in the biosynthesis of the anthocyanin class of flavonoids (Wilmouth et al. 2002).

Upon querying against the Arabidopsis proteome, four closely related homologs (UGT89B1, UGT89A2, UGT89C1, AT1G51210) were identified, with 73 predicted associated proteins in STRING with substantially enriched annotation and evidence diversity compared with the model legume Medicago network. The UGT89C1 network was particularly informative, identifying core flavonoid biosynthesis enzymes, including flavonol synthase/flavanone 3-hydroxylase (FLS1), chalcone isomerase (CHI1), chalcone synthase (CHS), flavanone 3'-hydroxylase (F3H), flavonoid 3'- monooxygenase (CYP75B1), rhamnose synthase (RHM1), and dihydroflavonol 4-reductase (DFRA), together with the transcription factors MYB75 and MYB111 (Table S6). These network predictions were used to identify genes that are co-expressed with *TpUGT89B1* in red clover rather than those that infer direct interactions for *TpUGT89B1*.

To determine whether these predicted co-expression partners were induced during *F. avenaceum* infection, we examined the Formica RNAseq dataset. Among the 50 most strongly induced genes unique to infected Formica, both *TpCYP75B1* and *TpCHS* were highly upregulated compared with those in non-infected Formica controls (Table S7). The red clover ortholog of *FLS1* was identified by BLASTP and included for RT—qPCR analysis because of its high confidence scores with UGT89 proteins in both Medicago and Arabidopsis networks. RT—qPCR analysis of infected and non-infected Formica roots at 7 dpi revealed that the expression of *TpUGT89B1* and the selected flavonoid biosynthesis pathway genes *TpCYP75B1*, *TpCHS* and *TpFLS1* significantly increased following fungal infection (Fig. S4; $P \leq 0.05$ or $P \leq 0.01$). The expression patterns of *TpCHS* and *TpCYP75B1* were consistent with the RNA-seq results, supporting the coordinated induction of *TpUGT89B1* and flavonoid biosynthesis genes during pathogen infection.

Discussion

The molecular basis of resistance to *F. avenaceum* in red clover remains largely unexplored. In this study, we compared the transcriptomic responses of contrasting red clover accessions following *F. avenaceum* infection to identify candidate genes associated with resistance. In total, 251 transcripts were identified as uniquely activated in the more resistant Formia accession compared with the highly susceptible SW 1678002. The strong induction of *RLKs* and *UGTs* in Formica is consistent with an integrated defense response involving pathogen perception and metabolic reprogramming (Pandey et al. 2016; Dievart et al. 2020; Jones et al. 2024). This may be particularly important in legumes, where immunity must restrict pathogens while permitting beneficial interactions with microorganisms such as nitrogen-fixing rhizobia (Cao et al. 2017; Martins et al. 2020).

Red clover lacks efficient transient assays and transformation procedures. This feature is typical for legumes that are well known to be recalcitrant to most transgenic technologies (Baloglu et al. 2022; Nivya and Shah 2023). Recent developments in soybean demonstrate that further improvements toward

faster and less genotype-dependent procedures are possible (Zhong et al. 2024). Among the approaches tested here, early transfer of young shoots from selection medium, which hampers their growth, to regeneration medium promoted shoot development and shortened the regeneration process, with positive shoots obtained within five weeks. The transformation efficiencies achieved for *TpUGT89B1* (4.6%) and *TpLRR-RLK* (6.6%) are within the range reported for other recalcitrant legumes (Kaur et al. 2022) and higher than those previously reported for different *Trifolium* species (Ding et al. 2003; Rojo et al. 2021; Jia et al. 2023). The outcrossing nature of red clover and its reliance on insect pollination make conventional transgenic cultivars unlikely to become commercial products, at least in Europe. Genome editing may provide future opportunities to modify disease susceptibility genes and other agronomically important loci, such as self-incompatibility alleles, and become important breeding materials.

Overexpression of either *TpUGT89B1* or *TpLRR-RLK* reduced disease symptoms and fungal colonization. Importantly, the stable transformation results were consistent with those obtained in the transient assays, supporting a role for both genes in restricting *F. avenaceum* growth and demonstrating the usefulness of transient expression for rapid screening of candidate genes. RLKs located at the plasma membrane participate in the recognition of extracellular signals and the initiation of downstream immune responses (Dievart et al. 2020; Jones et al. 2024). The activation of several RLK classes in resistant Formica, including LRR-RLKs, CRKs, LecRLKs and WAKs, suggests that cell-surface signaling is an important component of red clover's recognition of *F. avenaceum*.

The plant genomes contain large and diverse UGT families, with 122 members identified in Arabidopsis, 243 in Medicago, more than 400 in alfalfa, 208 in soybean, and 121 in red clover (Paquette et al. 2003; Wilson and Tian 2019; Krishnamurthy et al. 2020; Yu et al. 2022). Glycosyltransferases (GTs) are classified into 116 different families on the basis of sequence similarity (CAZy, http://www.cazy.org/GlycosylTransferase-family), and this number continues to increase as new members are identified. Of these, GTs utilizing UDP-conjugated carbohydrates as sugar donors are referred to as family 1 GTs and are generally cytosolic in nature (Bowles et al. 2006; Yonekura-Sakakibara and Hanada 2011). Plant Family 1 UGTs typically adopt a GT-B fold and contain a highly conserved plant secondary product glycosyltransferase (PSPG) motif at the C-terminus, which is involved in UDP-sugar donor recognition, whereas the more variable N-terminal region largely determines acceptor specificity (Gachon et al. 2005; Wang et al. 2009). This structural diversity enables UGTs to glycosylate phytohormones, specialized metabolites and xenobiotic compounds, thus altering their stability, solubility, localization and biological activity (Bowles et al. 2006; He et al. 2020; Mao et al. 2025). Depending on the available substrate and biological context, UGTs can either enhance or reduce defense responses by modifying defense-related metabolites or signaling molecules (Jiang et al. 2025; Zhao et al. 2025; Zhang et al. 2025). Our structural analysis supports the classification of TpUGT89B1 as a typical plant family 1 UGT. Although the predicted structure closely resembles the experimentally characterized rice UGT Os79, the modeling supports only its capacity for UDP-dependent glycosylation and does not identify its physiological substrate.

Protein interaction network analysis and RT–qPCR co-expression data provided an additional biological context for TpUGT89B1, linking it to flavonoid biosynthesis. Homology-based STRING analysis revealed that TpUGT89B1-related proteins were associated with flavonoid and phenylpropanoid pathways, and *TpUGT89B1* was co-induced with *TpCHS*, *TpCYP75B1*, and *TpFLS1* in *F. avenaceum*-infected Formica roots. CHS catalyzes the first committed step in flavonoid biosynthesis, whereas CYP75B1 and FLS function in downstream branches, leading to the production of diverse flavonoid compounds (Liu et al. 2021). Recent studies have shown that the activation of flavonoid biosynthesis is a dominant defense strategy in several plant–*Fusarium* interactions (Kumar et al. 2024; Yang et al. 2024). Although the STRING associations are based on homologous proteins rather than direct interactions, the co-expression data suggest that TpUGT89B1 is potentially associated with flavonoid-related defense metabolism.

The co-expression of TpUGT89B1 with flavonoid pathway genes may have implications for legume symbiosis. Flavonoids serve as key signals in the initiation of *Rhizobium* symbiosis in legumes, and components of the plant immune system are tightly integrated with symbiotic signaling (Cao et al. 2017). The balance between pathogen defense and symbiont accommodation in legumes is an active area of investigation, and a UGT modulating flavonoid glycosylation status could influence both processes (Cao et al. 2017; Martins et al. 2020). This dual context is a distinctive feature of legume biology that distinguishes immune studies in red clover from those in cereals.

Collectively, these results revealed that *TpUGT89B1* and *TpLRR-RLK* are defense genes that significantly restrict *F. avenaceum* colonization in red clover. *TpUGT89B1* resulted in the greatest reduction in fungal colonization, and structural modeling supported its classification as a plant family 1 UGT. Its co-expression with flavonoid biosynthesis genes during infection points to glycosylation and specialized metabolism as important defense components against *F. avenaceum*. Improved information concerning the red clover genome will hopefully assist in the identification of additional partners that interact with this important root pathogen in red clover.

Declarations

Acknowledgments

The authors acknowledge the SNP&SEQ Technology Platform in Uppsala for library preparation and RNA sequencing. The facility is part of the National Genomics Infrastructure (NGI) Sweden and Science for Life Laboratory. The SNP&SEQ Platform is also supported by the Swedish Research Council and the Knut and Alice Wallenberg Foundation. We thank the PDC Center for High Performance Computing at KTH Royal Institute of Technology, Sweden, for providing the computational resources used in this study. We also thank Elisabeth Lööf for assistance with the transient assays, Fredrik Dölfors for assistance with qRT-PCR analysis and Linda Öhlund (Lantmännen, Sweden) for providing the red clover seeds.

Funding

This work was supported by a grant from the Swedish University of Agricultural Sciences (SLU), and the Grogrund Initiative (SLU). AGD is supported by funding from the Novo Nordisk Foundation.

Conflict of interest The authors declare that they have no competing interests. The authors have no relevant financial or non-financial interests to disclose.

Authors' contributions

Experiments were designed and planned by SJ and CD. Work was conducted and data acquired by SJ. AGD performed structural modeling analyses. The manuscript was written and edited by SJ and CD. All authors read and approved the final manuscript.

Ethics approval statement

This study does not require any ethical approval.

References

1. Baloglu MC, Celik Altunoglu Y, Baloglu P et al (2022) Gene-editing technologies and applications in legumes: progress, evolution, and future prospects. Front Genet 13:859437. https://doi.org/10.3389/fgene.2022.859437
2. Bauer S, Mekonnen DW, Hartmann M, et al (2021) UGT76B1, a promiscuous hub of small molecule-based immune signaling, glucosylates N-hydroxypipecolic acid, and balances plant immunity. The Plant Cell 33:714–734. https://doi.org/10.1093/plcell/koaa044
3. Boutet E, Lieberherr D, Tognolli M et al (2016) UniProtKB/Swiss-Prot, the manually annotated section of the UniProt KnowledgeBase: how to use the entry view. In: Edwards D (ed) Plant bioinformatics: methods and protocols. Methods in Molecular Biology, vol 1374. Humana Press, New York, NY, pp 23–54. https://doi.org/10.1007/978-1-4939-3167-5_2
4. Bowles D, Lim EK, Poppenberger B et al (2006) Glycosyltransferases of lipophilic small molecules. Annu Rev Plant Biol 57:567–597. https://doi.org/10.1146/annurev.arplant.57.032905.105429
5. Cao Y, Halane MK, Gassmann W et al (2017) The role of plant innate immunity in the legume-rhizobium symbiosis. Annu Rev Plant Biol 68:535–561. https://doi.org/10.1146/annurev-arplant-042916-041030
6. Chakraborty S, Nguyen B, Wasti SD, et al (2019) Plant leucine-rich repeat receptor kinase (LRR-RK): structure, ligand perception, and activation mechanism. Molecules 24:3081. https://doi.org/10.3390/molecules24173081
7. ByteDance AML AI4Science Team, Chen X, et al (2025) Protenix-advancing structure prediction through a comprehensive AlphaFold3 reproduction. bioRxiv. https://doi.org/10.1101/2025.01.08.631967
8. De Vega JJ, Ayling S, Hegarty M et al (2015) Red clover (*Trifolium pratense* L.) draft genome provides a platform for trait improvement. Sci Rep 5:17394. https://doi.org/10.1038/srep17394

9. Di Tommaso P, Chatzou M, Floden EW et al (2017) Nextflow enables reproducible computational workflows. Nat Biotechnol 35:316–319. https://doi.org/10.1038/nbt.3820
10. Dievart A, Gottin C, Périn C et al (2020) Origin and diversity of plant receptor-like kinases. Annu Rev Plant Biol 71:131–156. https://doi.org/10.1146/annurev-arplant-073019-025927
11. Ding YL, Aldao-Humble G, Ludlow E et al (2003) Efficient plant regeneration and *Agrobacterium*-mediated transformation in *Medicago* and *Trifolium* species. Plant Sci 165:1419–1427.
12. Dobin A, Davis CA, Schlesinger F et al (2013) STAR: ultrafast universal RNA-seq aligner. Bioinformatics 29:15–21. https://doi.org/10.1093/bioinformatics/bts635
13. Ewels P, Magnusson M, Lundin S et al (2016) MultiQC: summarize analysis results for multiple tools and samples in a single report. Bioinformatics 32:3047–3048. https://doi.org/10.1093/bioinformatics/btw354
14. Gachon CM, Langlois-Meurinne M, Saindrenan P (2005) Plant secondary metabolism glycosyltransferases: the emerging functional analysis. Trends Plant Sci 10:542–549. https://doi.org/10.1016/j.tplants.2005.09.007
15. Gresshoff PM, Hayashi S, Biswas B et al (2015) The value of biodiversity in legume symbiotic nitrogen fixation and nodulation for biofuel and food production. J Plant Physiol 172:128–136. https://doi.org/10.1016/j.jplph.2014.05.013
16. Grundy EB, Gresshoff PM, Su H et al (2023) Legumes regulate symbiosis with rhizobia via their innate immune system. Int J Mol Sci 24:2800. https://doi.org/10.3390/ijms24032800
17. He Y, Wu L, Liu X et al (2020) *TaUGT6*, a novel UDP-glycosyltransferase gene enhances the resistance to FHB and DON accumulation in wheat. Front Plant Sci 11:574775. https://doi.org/10.3389/fpls.2020.574775
18. Inbaia S, Farooqi A, Ray RV (2023) Aggressiveness and mycotoxin profile of *Fusarium avenaceum* isolates causing *Fusarium* seedling blight and *Fusarium* head blight in UK malting barley. Front Plant Sci 14:1121553. https://doi.org/10.3389/fpls.2023.1121553
19. Jambagi S, Dixelius C (2023) A robust hydroponic-based system for screening red clover (*Trifolium pratense*) for *Fusarium avenaceum*. Legume Sci 5:e209. https://doi.org/10.1002/leg3.209
20. Jambagi S, Hodén KP, Öhlund L et al (2023) Red clover root-associated microbiota is shaped by geographic location and choice of farming system. J Appl Microbiol 134:lxad067. https://doi.org/10.1093/jambio/lxad067
21. Jia T, Tang T, Cheng B, et al (2023) Development of two protocols for *Agrobacterium*-mediated transformation of white clover (*Trifolium repens*) via the callus system. 3 Biotech 13:150. https://doi.org/10.1007/s13205-023-03591-2
22. Jiang D, Lin S, Xie L et al (2025) UDP-glycosyltransferase *PpUGT74F2* is involved in fruit immunity via modulating salicylic acid metabolism. Hortic Res 12:uhaf049. https://doi.org/10.1093/hr/uhaf049
23. Jones C, De Vega J, Lloyd D, et al (2020) Population structure and genetic diversity in red clover (*Trifolium pratense* L.) germplasm. Sci Rep 10:8364. https://doi.org/10.1038/s41598-020-64989-z

24. Jones JDG, Staskawicz BJ, Dangl JL (2024) The plant immune system: from discovery to deployment. Cell 187:2095–2116. https://doi.org/10.1016/j.cell.2024.03.045
25. Kaur R, Donoso T, Scheske C, et al (2022) Highly efficient and reproducible genetic transformation in pea for targeted trait improvement. ACS Agric Sci Technol 2:780–787. https://doi.org/10.1021/acsagscitech.2c00084
26. Krishnamurthy P, Tsukamoto C, Ishimoto M (2020) Reconstruction of the evolutionary histories of *UGT* gene superfamily in legumes clarifies the functional divergence of duplicates in specialized metabolism. Int J Mol Sci 21:1855. https://doi.org/10.3390/ijms21051855
27. Kumar GA, Kumar S, Bhardwaj R et al (2024) Recent advancements in multifaceted roles of flavonoids in plant-rhizomicrobiome interactions. Front Plant Sci 14:1297706. https://doi.org/10.3389/fpls.2023.1297706
28. Kundu A, Moraes TA, Price RJ et al (2025) Getting to the route: the evolution of nitrogen-fixing nodules. Annu Rev Cell Dev Biol 41:457–478. https://doi.org/10.1146/annurev-cellbio-101123-093247
29. Legume Phylogeny Working Group (2018) Legume phylogeny and classification. https://www.legumedata.org/working-groups/phylogenetics/
30. Li S, Cong Y, Liu Y et al (2017) Optimization of *Agrobacterium*-mediated transformation in soybean. Front Plant Sci 8:246. https://doi.org/10.3389/fpls.2017.00246
31. Lindström K, Mousavi SA (2020) Effectiveness of nitrogen fixation in rhizobia. Microb Biotechnol 13:1314–1335. https://doi.org/10.1111/1751-7915.13517
32. Lisciani S, Marconi S, Le Donne C et al (2024) Legumes and common beans in sustainable diets: nutritional quality, environmental benefits, spread and use in food preparations. Front Nutr 11:1385232. https://doi.org/10.3389/fnut.2024.1385232
33. Liu W, Feng Y, Yu S et al (2021) The flavonoid biosynthesis network in plants. Int J Mol Sci 22:12824. https://doi.org/10.3390/ijms222312824
34. Livak KJ, Schmittgen TD (2001) Analysis of relative gene expression data using real-time quantitative PCR and the $2^{-\Delta\Delta CT}$ method. Methods 25:402–408. https://doi.org/10.1006/meth.2001.1262
35. Love MI, Huber W, Anders S (2014) Moderated estimation of fold change and dispersion for RNA-seq data with DESeq2. Genome Biol 15:550. https://doi.org/10.1186/s13059-014-0550-8
36. Lysøe E, Harris LJ, Walkowiak S et al (2014) The genome of the generalist plant pathogen *Fusarium avenaceum* is enriched with genes involved in redox, signaling and secondary metabolism. PLoS ONE 9:e112703. https://doi.org/10.1371/journal.pone.0112703
37. Mao Y, Luo J, Cai Z (2025) Biosynthesis and regulatory mechanisms of plant flavonoids: a review. Plants 14:1847. https://doi.org/10.3390/plants14121847
38. Martin M (2011) Cutadapt removes adapter sequences from high-throughput sequencing reads. EMBnet J 17:10. https://doi.org/10.14806/ej.17.1.200

39. Martins D, Araujo SDS, Rubiales D et al (2020) Legume crops and biotrophic pathogen interactions: a continuous cross-talk of a multilayered array of defense mechanisms. Plants 9:1460. https://doi.org/10.3390/plants9111460
40. Mehdi Khanlou K, Van Bockstaele E (2012) A critique of widely used normalization software tools and an alternative method to identify reliable reference genes in red clover (*Trifolium pratense* L.). Planta 236:1381–1393. DOI 10.1007/s00425-012-1682-2
41. Ngou BPM, Ding P, Jones JDG (2022) Thirty years of resistance: zig-zag through the plant immune system. The Plant Cell 34:1447–1478. https://doi.org/10.1093/plcell/koac041
42. Nielsen LK, Cook DJ, Edwards SG et al (2014) The prevalence and impact of *Fusarium* head blight pathogens and mycotoxins on malting barley quality in UK. Int J Food Microbiol 179:38–49. https://doi.org/10.1016/j.ijfoodmicro.2014.03.023
43. Nivya VM, Shah JM (2023) Recalcitrance to transformation, a hindrance for genome editing of legumes. Front Genome Ed 5:1247815. https://doi.org/10.3389/fgeed.2023.1247815
44. Nuc K, Olejnik P (2025) Molecular mechanisms underlying root nodule formation and activity. Agronomy 15:1552. https://doi.org/10.3390/agronomy15071552
45. Pandey D, Rajendran SRCK, Gaur M et al (2016) Plant defense signaling and responses against necrotrophic fungal pathogens. J Plant Growth Regul 35:1159–1174. https://doi.org/10.1007/s00344-016-9600-7
46. Paquette S, Møller BL, Bak S (2003) On the origin of family 1 plant glycosyltransferases. Phytochem 62:399–413. DOI 10.1016/S0031-9422(02)00558-7
47. Patro R, Duggal G, Love MI et al (2017) Salmon provides fast and bias-aware quantification of transcript expression. Nat Methods 14:417–419. https://doi.org/10.1038/nmeth.4197
48. Poole P, Ramachandran V, Terpolilli J (2018) Rhizobia: from saprophytes to endosymbionts. Nat Rev Microbiol 16:291–303. https://doi.org/10.1038/nrmicro.2017.171
49. Rajkumari J, Katiyar P, Dheeman S et al (2022) The changing paradigm of rhizobial taxonomy and its systematic growth up to postgenomic technologies. World J Microbiol Biotechnol 38:206. https://doi.org/10.1007/s11274-022-03370-w
50. Rojo FP, Seth S, Erskine W et al (2021) An improved protocol for *Agrobacterium*-mediated transformation in subterranean clover (*Trifolium subterraneum* L.). Int J Mol Sci 22:4181. https://doi.org/10.3390/ijms22084181
51. Schultze M, Kondorosi A (1998) Regulation of symbiotic root nodule development. Annu Rev Genet 32:33–57. https://doi.org/10.1146/annurev.genet.32.1.33
52. Szklarczyk D, Nastou K, Koutrouli M et al (2025) The STRING database in 2025: protein networks with directionality of regulation. Nucleic Acids Res 53:D730–D737. https://doi.org/10.1093/nar/gkae1113
53. Thapa G, Gunupuru LR, Hehir JG et al (2018) A pathogen-responsive leucine rich receptor like kinase contributes to *Fusarium* resistance in cereals. Front Plant Sci 9:867. https://doi.org/10.3389/fpls.2018.00867

54. Valujeva K, Grinfelde I, Pilecka-Ulcugaceva J et al (2025) The role of red clover (*Trifolium pratense* L.) in mitigating greenhouse gas emissions: insights from a temperate agricultural ecosystem. Agric Ecosyst Environ 393:109779. https://doi.org/10.1016/j.agee.2025.109779
55. Van Bel M, Proost S, Wischnitzki E et al (2012) Dissecting plant genomes with the PLAZA comparative genomics platform. Plant Physiol 158:590–600. https://doi.org/10.1104/pp.111.189514
56. he X (2009) Structure, mechanism and engineering of plant natural product glycosyltransferases. FEBS Lett 583:3303–3309. https://doi.org/10.1016/j.febslet.2009.09.042
57. Wetterhorn KM, Newmister SA, Caniza RK et al (2016) Crystal structure of Os79 (Os04g0206600) from *Oryza sativa*: a UDP-glucosyltransferase involved in the detoxification of deoxynivalenol. Biochem 55:6175–6186. https://doi.org/10.1021/acs.biochem.6b00709
58. Wilmouth RC, Turnbull JJ, Welford RW et al (2002) Structure and mechanism of anthocyanidin synthase from *Arabidopsis thaliana*. Structure 10:93–103.
59. Wilson AE, Tian L (2019) Phylogenomic analysis of UDP-dependent glycosyltransferases provides insights into the evolutionary landscape of glycosylation in plant metabolism. The Plant J 100:1273–1288. https://doi.org/10.1111/tpj.14514
60. Xue AG, Chen Y, Seifert K et al (2019) Prevalence of *Fusarium* species causing head blight of spring wheat, barley and oat in Ontario during 2001–2017. Can J Plant Pathol 41:392–402. https://doi.org/10.1080/07060661.2019.1582560
61. Yang K, Zhou G, Chen C et al (2024) Joint metabolomic and transcriptomic analysis identify unique phenolic acid and flavonoid compounds associated with resistance to *Fusarium* wilt in cucumber (*Cucumis sativus* L.). Front Plant Sci 15:1447860. https://doi.org/10.3389/fpls.2024.1447860
62. Ye J, Coulouris G, Zaretskaya I et al (2012) Primer-BLAST: a tool to design target-specific primers for polymerase chain reaction. BMC Bioinformatics 13:134. https://doi.org/10.1186/1471-2105-13-134
63. Yonekura-Sakakibara K, Hanada K (2011) An evolutionary view of functional diversity in family 1 glycosyltransferases. The Plant J 66:182–193. https://doi.org/10.1111/j.1365-313X.2011.04493.x
64. Yu A, Jiang X, Sun Y et al (2022) Genome-wide identification, characterization, and expression analysis of UDP-glycosyltransferase genes associated with secondary metabolism in alfalfa (*Medicago sativa* L.). Front Plant Sci 13:1001206. https://doi.org/10.3389/fpls.2022.1001206
65. Zhang W, Cheng Y, Shao L et al (2025) The glycosylation status of small molecules impacts different aspects of plant immunity. Physiol Plant 177:e70292. https://doi.org/10.1111/ppl.70292
66. Zhao S, Dong G, Liu C et al (2025) Two pathogen-inducible UDP-glycosyltransferases, UGT73C3 and UGT73C4, catalyze the glycosylation of pinoresinol to promote plant immunity in *Arabidopsis*. Plant Commun 6:101261. https://doi.org/10.1016/j.xplc.2025.101261
67. Zhong H, Li C, Yu W et al (2024) A fast and genotype-independent in planta *Agrobacterium*-mediated transformation method for soybean. Plant Commun 5:101063. https://doi.org/10.1016/j.xplc.2024.101063

Figures

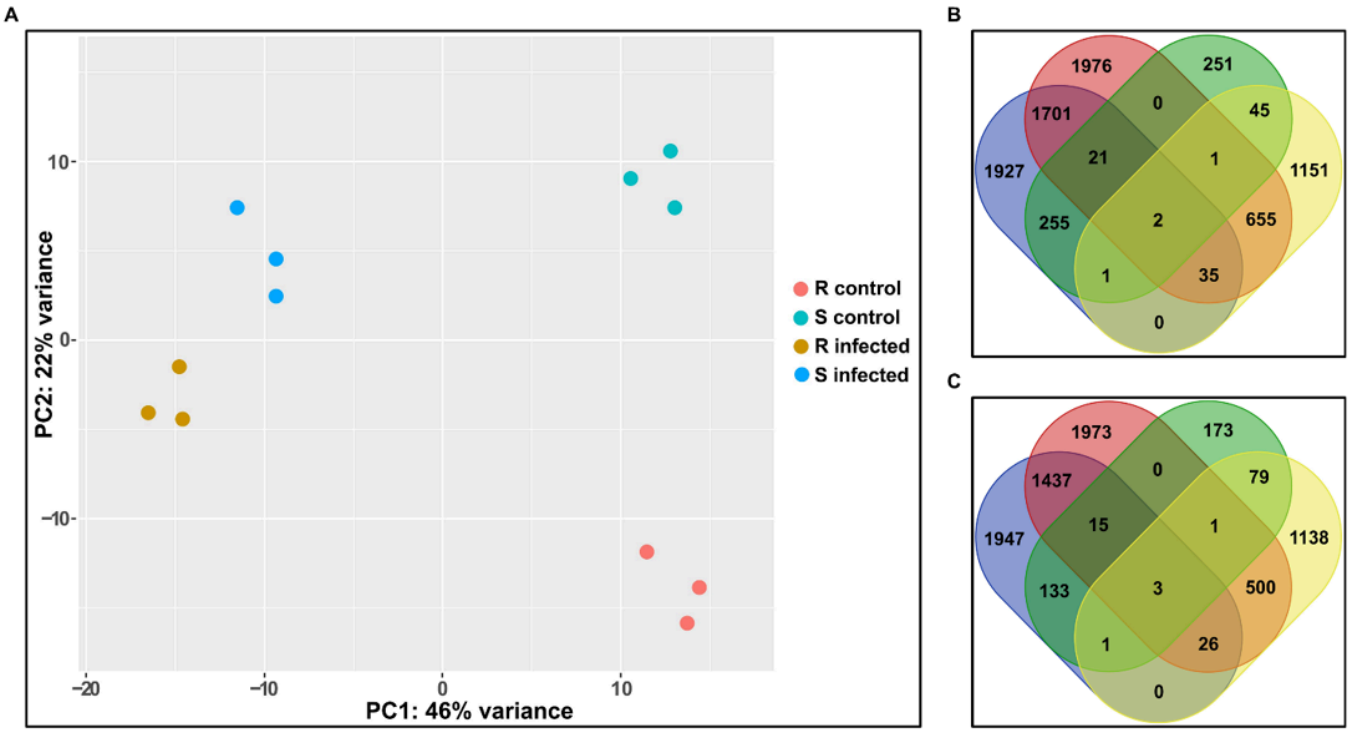


Figure 1

Transcriptomic profiling of *F. avenaceum*-infected and non-infected resistant (R) and susceptible (S) red clover. **A** Principal component analysis of normalized transcript abundance values across three biological replicates per treatment for both infected and non-infected (control) R and S accessions. Venn diagrams of **B** upregulated and **C** downregulated differentially expressed genes (DEGs; $\log_2$fold change > 1, $P < 0.01$) that were shared or unique among the four comparison groups. Color ID: blue; Formica infected vs. non-infected, red; SW 1678002 infected vs. non-infected, green; Formica infected vs. SW 1678002 infected, yellow; Formica non-infected vs. SW 1678002 non-infected. Overlapping regions contain DEGs shared between each comparison; non-overlapping regions represent unique DEGs.

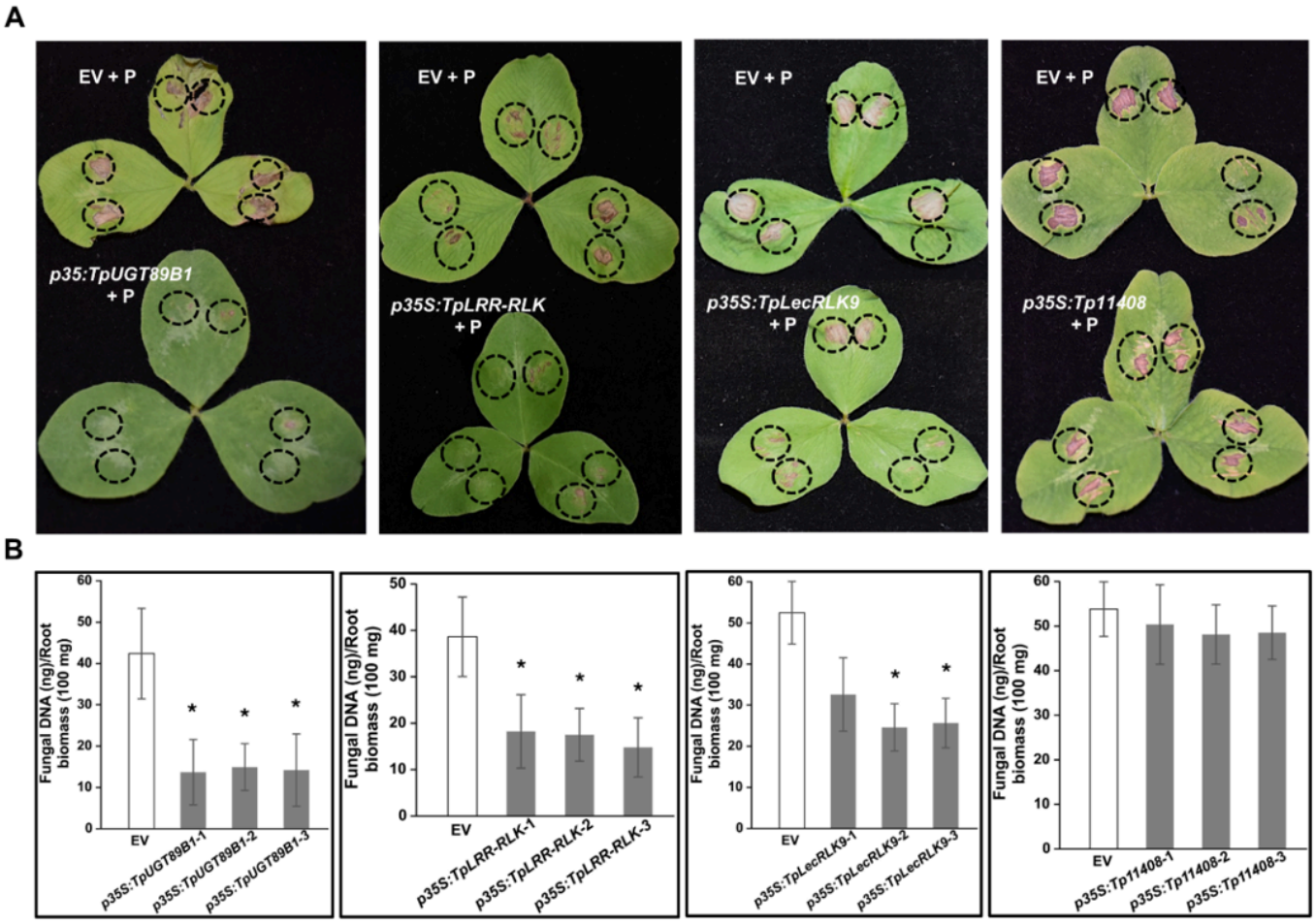


Figure 2

Transient expression assay of candidate defense genes in red clover leaves challenged with *F. avenaceum*. **A** Disease phenotype of red clover leaves infiltrated with *Agrobacterium* AGL1 carrying *p35S:TpUGT89B1*, *p35S:TpLRR-RLK*, *p35S:TpLecRLK9* or *p35S:Tp11408*, followed by inoculation with *F. avenaceum* (50 µl, 10^6 spores/ml). Images were taken at 5 dpi. EV, empty vector control; P, pathogen-inoculated; dotted circle, agroinfiltrated zone. **B** Quantification of *F. avenaceum* DNA in agroinfiltrated leaves at 5 dpi using qPCR. The error bars represent the means ± SDs. Asterisks indicate significant differences compared with the empty vector control ($P \leq 0.05$). Statistical analysis was performed with a Student's *t* test with three biological replicates.

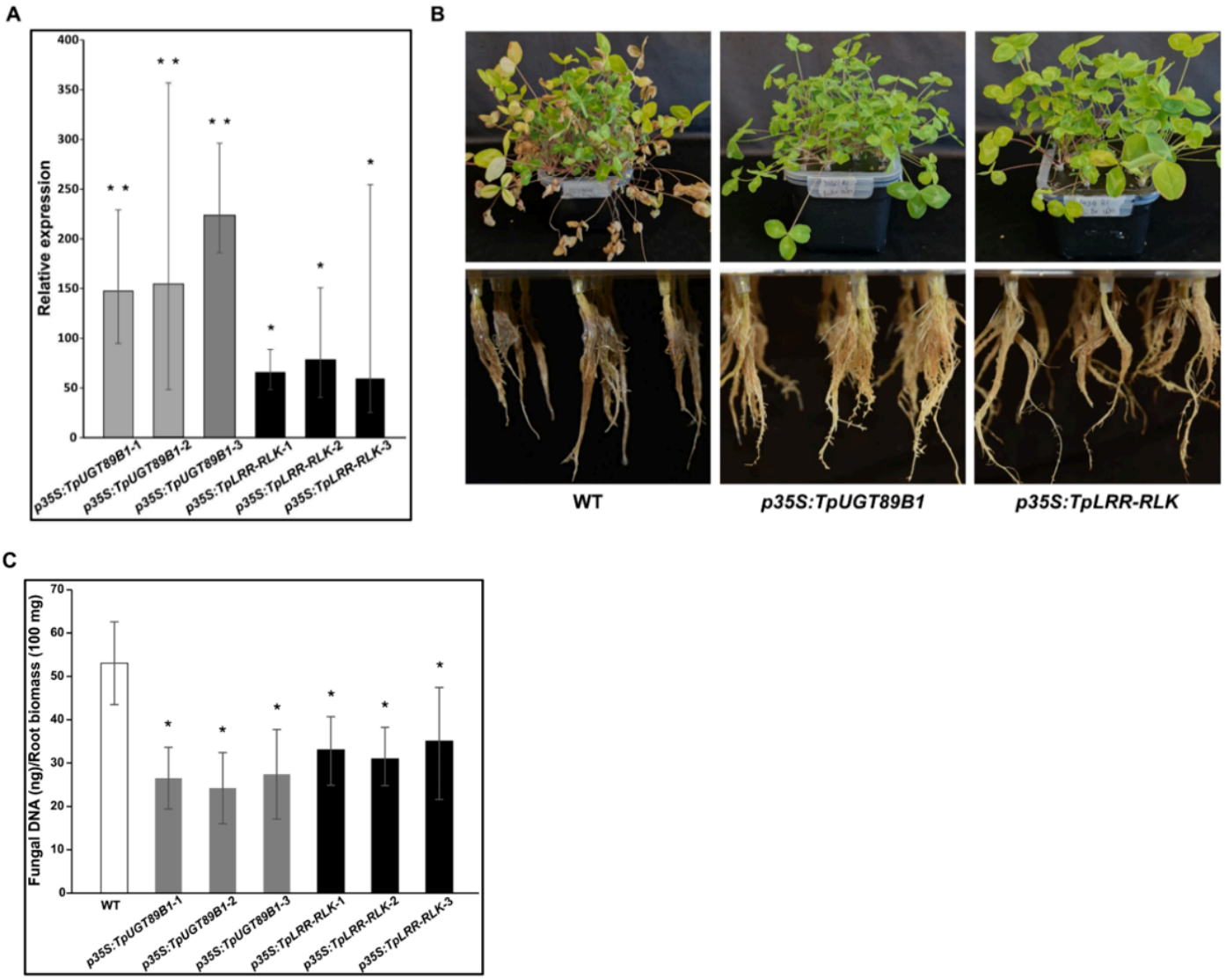


Figure 3

Analysis of *p35S:TpUGT89B1* and *p35S:TpLRR-RLK* in transgenic red clover plants. **A** RT—qPCR analysis of the independent transgenic lines (*p35S:TpUGT89B1*-1, 2, 3 and *p35S:TpLRR-RLK*-1, 2, 3). The data are relative to susceptible red clover SW 1678002 wildtype (WT) roots (control value =1) and normalized to the *translation initiation factor* (*EIF-4α*) expression levels. The data were analyzed using the $2^{-\Delta\Delta CT}$ method. **B** Phenotypes of four-week-old hydroponically grown SW 1678002 (WT), *p35S:TpUGT89B1* and *p35S:TpLRR-RLK* plants at 7 dpi with *F. avenaceum* (~30,000 spores/ml) showing root and foliar symptoms. **C** Quantification of *F. avenaceum* DNA in the roots of WT and transgenic plants at 7 dpi using qPCR. The bar chart includes the means ± SDs (n=3 biological replicates). Asterisks indicate significant differences according to Student's *t* test (*$P \leq 0.05$, ** $P \leq 0.01$) compared with the WT.

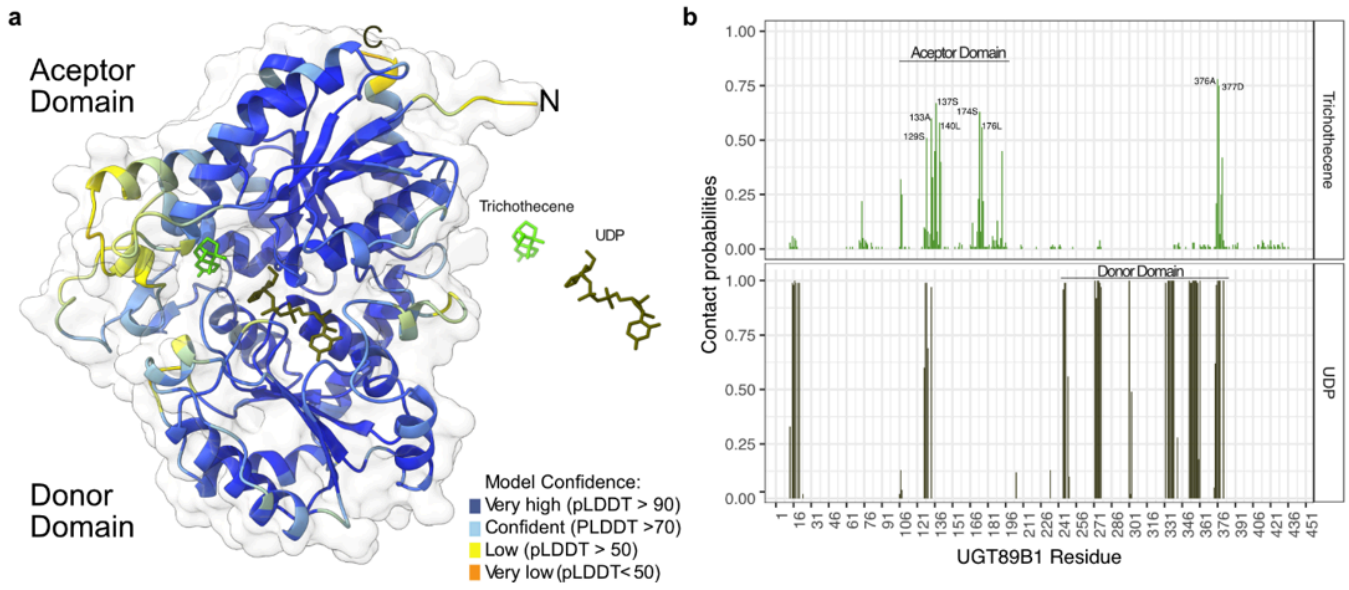


Figure 4

Structural model of TpUGT89B1 and predicted ligand-binding regions. **A** Predicted structure of TpUGT89B1 in complex with the UDP-sugar analogU2F (olive green) and the reference trichothecene ligand 7E0 (bright green) generated using Protenix-v0.5.0. The protein is colored (dark blue, cyan, yellow and orange) according to the pLDDT confidence score (dark blue (highest confidence) to orange (lowest confidence) with the predicted N-terminal acceptor-binding region for accommodating the reference ligand 7E0 and the C-terminal donor-binding region predicted to recognize the UDP-sugar donor. Structural visualization was performed using UCSF ChimeraX version 1.3. **B**Predicted contact probabilities between individual amino acid residues of TpUGT89B1 and the reference trichothecene ligand 7E0 (top) or U2F (bottom). Higher peaks indicate residues with a greater probability of contacting the ligand.

Supplementary Files

This is a list of supplementary files associated with this preprint. Click to download.

- SupplementaryInformationFiguresS1S4TablesS1S7.docx
- Supplementarydatafile1ProtenixPDBbasedmultiplesequencealignmentoutputforTpUGT89B1.xlsx
- SupplementaryInformation.docx